THE JOURNAL OF BIOLOGICAL CHEMISTRY
Vol. 278, No. 15, Issue of April 11, pp. 13333–13341, 2003

Printed in U.S.A.

Structural Basis of Calcification Inhibition by α_2-HS Glycoprotein/Fetuin-A

FORMATION OF COLLOIDAL CALCIPROTEIN PARTICLES*

Received for publication, October 24, 2002, and in revised form, January 29, 2003
Published, JBC Papers in Press, January 29, 2003, DOI 10.1074/jbc.M210868200

Alexander Heiss‡, Alexander DuChesne§, Bernd Denecke‡, Joachim Grötzinger¶, Kazuhiko Yamamoto‖, Thomas Renné, and Willi Jahnen-Dechent‡ ‡‡**

*From ‡IZKF BIOMAT, University Clinics, RWTH Aachen, Pauwelsstrasse 30, D-52074 Aachen, Germany, §Max-Planck-Institute for Polymer Research, Ackermannweg 10, D-55128 Mainz, Germany, ¶Institute of Biochemistry, University of Kiel, Olshausenstrasse 40, D-24098 Kiel, Germany, ‖Department of Biochemistry, Kinki University School of Medicine, Osaka 589-8511, Japan, and **Institute for Clinical Biochemistry and Pathobiochemistry, Josef-Schneider-Strasse 2, Julius-Maximilians-University, D-97080 Würzburg, Germany*

Genetic evidence from mutant mice suggests that α_2-HS glycoprotein/fetuin-A (Ahsg) is a systemic inhibitor of precipitation of basic calcium phosphate preventing unwanted calcification. Using electron microscopy and dynamic light scattering, we demonstrate that precipitation inhibition by Ahsg is caused by the transient formation of soluble, colloidal spheres, containing Ahsg, calcium, and phosphate. These "calciprotein particles" of 30–150 nm in diameter are initially amorphous and soluble but turn progressively more crystalline and insoluble in a time- and temperature-dependent fashion. Solubilization in Ahsg-containing calciprotein particles provides a novel conceptual framework to explain how insoluble calcium precipitates may be transported and removed in the bodies of mammals. Mutational analysis showed that the basic calcium phosphate precipitation inhibition activity resides in the amino-terminal cystatin-like domain D1 of Ahsg. A structure-function analysis of wild type and mutant forms of cystatin-like domains from Ahsg, full-length fetuin-B, histidine-rich glycoprotein, and kininogen demonstrated that Ahsg domain D1 is most efficient in inhibiting basic calcium phosphate precipitation. The computer-modeled domain structures suggest that a dense array of acidic residues on an extended β-sheet of the cystatin-like domain Ahsg-D1 mediates efficient inhibition.

The combination of mineral with an organic matrix called "biomineral" is commonplace in biology. Biominerals studied in detail include magnetic crystals in bacteria (1), silica skeletons in diatomeous algae (2, 3), shells of marine molluscs (4, 5), and skeletons of vertebrate animals (6). Generally, biominerals form in close proximity with biomacromolecules. Ultrastructural analyses suggest that a protein scaffold provides the ordered and spatially restrained framework for crystal deposition. In mammals, collagen is an excellent scaffold for calcification. Noncollagenous proteins control nucleation, growth, shape, and orientation of crystals in the mineral phase (7, 8). Major mineral ions are equally distributed in the extracellular space of most living organisms. Extracellular fluids are especially supersaturated with regard to calcium and phosphate ions. Therefore, it is surprising that mineralization is restricted to collagenous matrix of the vertebrate skeleton and that once started mineralization does not proceed throughout the organism (9). This suggests that the inhibition of unwanted mineralization is at least as important as the initiation of mineralization. Genetic experimentation with mutant mice indeed suggests that mineralization is the default pathway, which must be actively prevented, not started (10). Unwanted mineralization resulted from the genetic ablation of mineralization inhibitors, pyrophosphate (11, 12) and matrix γ-carboxyl glutamic acid (GLA)[1]-containing protein (MGP) (13). We showed that the lack of α_2-HS glycoprotein/fetuin-A (Ahsg) results in severe systemic calcification in mice and humans (15).[2] Of note, Ahsg is the only protein inhibitor of calcification known so far that is systemic and present throughout the extracellular space in mammals. Due to its high affinity for the mineral phase of bone, Ahsg accumulates about 100-fold over other serum proteins in bones and teeth (16). This seems paradoxical, considering that Ahsg is an efficient inhibitor of calcification both *in vitro* and *in vivo*. Here we studied how Ahsg inhibits the formation of basic calcium phosphate (BCP). Using electron microscopy and dynamic light scattering, we determined that the inhibition is effected by a transient formation of colloidal spheres containing Ahsg, calcium, and phosphate, which we call "calciprotein particles." Further, the structure-function relationship of recombinant forms of Ahsg-like proteins from the cystatin superfamily, fetuin-B (FETUB), histidine-rich glycoprotein (HRG), and kininogen (KNG) suggests that the inhibition of unwanted calcification by Ahsg involves binding of BCP nuclei to an array of acidic amino acid residues on an extended β-sheet of the cystatin-like Ahsg domain D1. We suggest that the resulting diffusion barrier limits further growth of the

* This work was supported by a grant from the Deutsche Forschungsgemeinschaft (to W. J-D.). The costs of publication of this article were defrayed in part by the payment of page charges. This article must therefore be hereby marked "*advertisement*" in accordance with 18 U.S.C. Section 1734 solely to indicate this fact.

‡‡ To whom correspondence should be addressed: IZKF BIOMAT, University Clinics, Pauwelsstrasse 30, D-52074 Aachen, Germany. Tel.: 49-241-80-80163; Fax: 49-241-80-82573; E-mail: willi.jahnen@rwth-aachen.de.

[1] The abbreviations used are: GLA, γ-carboxyl glutamic acid; MGP, matrix GLA-containing protein; Ahsg, α_2-HS glycoprotein/fetuin-A; BCP, basic calcium phosphate; bAhsg and mAhsg, bovine and mouse Ahsg, respectively; BSA, bovine serum albumin; TEM, transmission electron microscopy; FETUB, fetuin-B; hFETUB and mFETUB, human and mouse FETUB, respectively; HRG, histidine-rich glycoprotein; hHRG, human HRG; KNG, kininogen; hKNG, human KNG; MBP, maltose-binding protein; GST, glutathione S-transferase; HS, α_2-Heremans-Schmid.

[2] C. Schäfer, A. Heiss, A. Schwarz, R. Westenfeld, M. Ketteler, J. Floege, W. Müller-Esterl, T. Schinke, and W. Jahnen-Dechent, submitted for publication.

crystal nuclei and thus delays their precipitation. This proposed mechanism of the transient inhibition of BCP precipitation by Ahsg is fundamentally different from previous concepts, namely sequestration of calcium ions by negatively charged proteins like serum albumin or calcium binding through an EF-hand motif.

EXPERIMENTAL PROCEDURES

Precipitation Inhibition Assay—The precipitation inhibition assay was performed as described (17). Briefly, a buffered salt solution (50 mM Tris/HCl, pH 7.4, 4.8 mM $CaCl_2$, 2×10^6 cpm of $[^{45}Ca]Cl_2$, 1.6 mM Na_2HPO_4) containing test proteins as indicated in the figure legends was incubated at 37 °C for 90 min. Precipitates were collected by centrifugation (15,000 × *g*, 5 min at room temperature), dissolved in 1% acetic acid, and quantified by liquid scintillation counting. All incubations were done in triplicates. Bovine serum albumin (BSA; Roth, Karlsruhe, Germany) and bovine fetuin/bAhsg (Sigma) were used as negative and positive control proteins, respectively.

Electron Microscopy and Electron Spectroscopy—For scanning electron microscopy, a supersaturated solution of calcium (2.5 mM $CaCl_2$) and phosphate (1.8 mM KH_2PO_4) was prepared (18) with and without 200 nM bAhsg added. After a 90-min incubation at 22 °C, precipitate was spun down, air-dried, and viewed in a Leo series 1400 scanning electron microscope (Leo Electron Microscopy Ltd., Cambridge, UK).

For transmission electron microscopy (TEM) analysis, bAhsg and BSA were purified by gel filtration (Superdex 200; Amersham Biosciences, Freiburg, Germany) in 50 mM Tris/HCl, pH 7.4. Monomer-containing fractions were collected, and the protein concentration was determined using a dye assay (Roti-Nanoquant, Roth, Karlsruhe, Germany). All solutions were microfiltered (0.22 μm) before mixing. Following the precipitation reaction in buffer (5 mM $CaCl_2$, 3 mM Na_2HPO_4, 50 mM Tris/HCl) at pH 7.4 and 22 and 37 °C, respectively, samples were dialyzed against water (MilliQ; Millipore Corp.) using micro dialysis cartridges. This step was essential for electron microscopy of the precipitation mixture, which would otherwise have been obscured by dried salt. The dialyzed samples were cleared by centrifugation for 1 min at 1000 × *g*. The supernatant and, if formed, the precipitate were transferred to carbon-coated grids. Excess liquid was blotted from the side. The samples were viewed directly in TEM without staining. Supporting films of 7-nm thickness were coated onto freshly cleaved mica using a Balzers BAE 250 vacuum evaporator (Bingen, Germany), floated onto water, and transferred to 300-mesh copper grids. For elemental mapping of carbon, supporting films were made of boron. Energy-filtering transmission electron microscopy was performed on a Leo 912 Omega instrument (tungsten filament) operated at 120 kV using an objective aperture of 16.5 millirads. The width of the energy window controlled by the opening of the energy selector slit was 10 eV. All images were recorded using a slow scan CCD camera (lateral resolution 1024 × 1024 pixels, 14-bit gray) and processed using a SIS-AnalySIS® image processing system. Elemental distribution images where all obtained by three window potential background extrapolation (19).

Dynamic Light Scattering—Dynamic light scattering was measured using a laser (Spectra Physics 165, $\lambda = 514$ nm, 300 milliwatts). The scattered intensity was recorded at $Q = 90°$ (VV geometry) and analyzed by an ALV 5000 autocorrelator. The square light scattering cell was equilibrated to $T = 20$ °C. Two-exponential fitting gave the best accuracy for all autocorrelation functions. The intensities given are the absolute intensities due to scattering of the corresponding component. The scattering intensity caused by pure water and the cell was approximately 7 kHz (toluene standard 55 kHz).

Molecular Modeling—A total of nine cystatin-like protein domains of fetuin-A/Ahsg, fetuin-B (FETUB), kininogen (KNG), and histidine-rich glycoprotein (HRG) were modeled comparatively. The models were generated with Modeler4 software (20) using chicken egg white cystatin (Protein Data Bank accession code 1CEW) (21) as a template structure. During iterative refinement steps, the generated models were evaluated with Procheck and Prosa II (20, 22, 23). Additionally, models were scrutinized for structural clashes by Ramachandran plotting. No ψ and ϕ angles that are located in the forbidden areas of the Ramachandran plot and no unnatural bond lengths were observed. All structures proposed formed a compact core. Energetically intolerable interactions between C-β atoms did not occur.

Recombinant Proteins—The cloning, expression, and purification of fusion proteins with maltose-binding protein (MBP) has been described (17). Full-length mAhsg cDNA and deletion mutants thereof were PCR-amplified and ligated into pRSET-5c vector containing a Myc tag sequence and an additional *Eco*RI site downstream of the cloning sequence. The Myc tag oligonucleotides used for vector modification are listed in Table I. Using PCR and the primers listed in Table I, Myc-tagged deletion mutants of mAhsg cDNA were generated and subcloned by *Bam*HI/*Eco*RI restriction/ligation into the vector pGEX-2T (Amersham Biosciences) for the expression of GST fusion proteins and by *Bam*HI/*Hin*dIII restriction/ligation into the vector pMAL-c2 (New England Biolabs, Schwalbach, Germany) for MBP fusion protein expression. Fetuin-B cDNA was cloned by reverse transcription-PCR from rat, mouse, and human liver mRNA using murine leukemia virus reverse transcriptase (PerkinElmer Life Sciences) and *Pwo* polymerase (PeqLab, Erlangen, Germany) into the vector pGEMT (Promega, Madison, WI). For fusion protein expression, the cDNA inserts were excised by *Bam*HI/*Eco*RI restriction and ligated into the vectors pGEX-2T and pMAL-c2. Using primer mutagenesis, serine residues Ser^{120}, Ser^{291}, Ser^{294}, and Ser^{296} of the mature mouse Ahsg protein chain were mutated to glutamic acid in order to mimic Ser phosphorylation at these sites (24, 25). Mutations were achieved by a three-step overlapping PCR using the primer pairs detailed in Table I. The mutated mAhsg was ligated into the vector pGEX-2T for subsequent expression as GST fusion protein (GST-mAhsg/4S>E). Table I lists the mutated mAhsg constructs and the PCR primers used for their construction.

To clone the cDNA sequences encoding cystatin-domains D1, D2, and D3 of human kininogen, total RNA was prepared from HepG2 cells following established protocols. The cystatin domains were cloned by reverse transcription-PCR using murine leukemia virus reverse transcriptase (New England Biolabs), *Taq* polymerase (Amersham Biosciences), and the primer pairs listed in Table I. Primers contained additional restriction sites and stop codons. The amplicons were ligated into vector pMAL-c2 using *Bam*HI/*Hin*dIII (hKNG-D1), *Xba*I/*Hin*dIII (hKNG-D2), or *Xba*I/*Pst*I (hKNG-D3), respectively.

All cloning steps were verified by DNA sequencing. Expressed proteins were probed on the protein level using species-specific antisera and immunoblotting. Specific antisera at our disposal were originally raised against human, rat, mouse, and bovine Ahsg and recombinant human, rat, and mouse FETUB (data not shown).

Protein Expression, Purification, and Refolding—Bacterial cultures were inoculated from an overnight preculture 1:500. At an A_{600} of 0.5, isopropyl-1-thio-β-D-galactopyranoside was added to a final concentration of 300 μM. After a 2-h incubation at 37 °C, the bacteria were harvested by centrifugation for 10 min at 2500 × g. The bacterial pellet was resuspended in buffer containing 20 mM Tris, pH 7.4, 1 mM EDTA, and 200 mM NaCl (MBP fusion protein, amylose column buffer) or in PBS (GST fusion protein, glutathione-Sepharose column buffer). In the case of small MBP-fused fragments of Ahsg D1, the salt concentration was adjusted to 300 mM to improve amylose binding. The suspension was frozen overnight at −20 °C. The thawed ice-cold suspension was pulse-sonicated three times for 20 s. Then 1% Triton-X100, a protease inhibitor mixture, DNase, and RNase to a final concentration 10 μg/ml were added, and the suspension was mixed for 10 min at 4 °C. Nuclease digestion of crude protein preparations was critically important for the reproducibility of precipitation assays, because DNA and RNA are potent inhibitors of BCP precipitation (26). Protein preparations, which proved active in the BCP precipitation inhibition assay, were routinely treated with proteinase K to ensure that the inhibitory activity indeed resided with the protein fraction of each preparation and not with residual contaminating nucleic acids or low molecular weight inhibitors.

After centrifugation for 15 min at 4 °C and 30,000 × *g*, the supernatant was loaded onto an amylose column. After washing the column with 3 column volumes of amylose column buffer for MBP fusion proteins and with 3 column volumes of PBS for GST fusion proteins, the MBP-fused proteins were eluted with amylose column buffer containing 10 mM maltose, and the GST-fused protein was eluted with buffer containing 20 mM Tris, pH 8, and 10 mM reduced glutathione.

Recombinant protein isolated from the bacteria without a denaturation/refolding cycle was generally inactive in the BCP precipitation inhibition assay. Therefore, every recombinant protein had to be denatured and refolded (17). The stability and activity of the fusion proteins depended on the refolding procedure. Following is an optimized refolding procedure yielding active protein for both GST and MBP fusion proteins.

All recombinant proteins were solubilized for 2 h at room temperature in a buffer containing 50 mM Tris/HCl adjusted to pH 8, 6 M urea, and 50 mM dithiothreitol. The denatured protein solution was concentrated to 5 mg/ml using the same buffer with dithiothreitol content reduced to 5 mM. Refolding was initiated by slow dilution of protein

TABLE I

Oligonucleotide primers used for cloning of cystatin domain-containing fusion proteins of GST or MBP and mouse Ahsg, mouse, rat, and human FETUB, and human KNG

Construct	5′-primer	3′-primer
Myc tag blunt/EcoR1	GGGGAGCAGAAGCTGATCTCGGAGGAGGACCTGAACTAG	
Myc tag EcoR1/blunt	AATTCTAGTTCAGGTCCTCCTCCGAGATCAGCTTCTGCTCCCC	
pRSET mAhsg-Myc	GGGCTGCCATATGGCTCCACAAGGTACAGG	GATTTTGAAGTGTCTGATCC
pMAL mAhsg-Myc	GGAGATATAGGATCCGCTCCACAAGGTACAGG	GCCAACTCAGCTTCCTTTCG
pGEX mAhsg-Myc	GGAGATATAGGATCCGCTCCACAAGGTACAGG	GCCAACTCAGCTTCCTTTCG
pGEX-mAhsg/4S>E-Myc	GAGTTTCTCCCTCGGCCTCCTCCACCTCGGCCAC	GTAATACGACTCACTATAGGGC
	AATTAACCCTCACTAAAGGG	CCAGACGAGGCAGAGGAC
	GTAATACGACTCACTATAGGGC	AATTAACCCTCACTAAAGGG
pRSET mAhsg 15–70-Myc	GAGAATTGCATATGGATGATCCAGAAGC	AGTGGTCTCCAGTGTGTC
pGEX-mAhsg 15–70-Myc	GGAGATATAGGATCCGATGATCCAGAAGC	GCCAACTCAGCTTCCTTTCG
pRSET mAhsg 1–81-Myc	GGGCTGCCATATGGCTCCACAAGGTACAGG	GTTTGGCAGCGGGGTGGG
pGEX mAhsg 1–81-Myc	GGAGATATAGGATCCGCTCCACAAGGTACAGG	GCCAACTCAGCTTCCTTTCG
pRSET mAhsg 42–81-Myc	GGATTCAAACATATGTTGAATCAGATCG	GTTTGGCAGCGGGGTGGG
pGEX mAhsg 42–81-Myc	GGAGATATAGGATCCTTGAATCAGATCG	GCCAACTCAGCTTCCTTTCG
pRSET mAhsg 42–70-Myc	GGATTCAAACATATGTTGAATCAGATCG	AGTGGTCTCCAGTGTGTC
MBP-mAhsg 42–70-Myc	GGAGATATAGGATCCTTGAATCAGATCG	GCCAACTCAGCTTCCTTTCG
GST-mFETUB	CCCTCTCACCTCTGCATCCGGGAT	GGAATTCTCAGGGTGGGACCAG
MBP-mFETUB	CCCTCTCACCTCTGCATCCGGGAT	GGAATTCTCAGGGTGGGACCAG
GST-rFETUB	CGGGATCCTTCGCACCTCTGCGTCC	GGAATTCAGGGGGTTCTTTGCTTTTC
GST-hFETUB	CGGGATCCCTCAACCCCTCGGCTC	GGAATTCTCATGGCGGAAGGACAAG
MBP-hKNG-domain D1	GTGGATCCCAGGAATCACAGTCCG	CAAGCTTCTAGGCTGGAGTAATCTG
MBP-hKNG-domain D2	GTCTAGACCAGCCGAGGGCCCTGTG	AAAGCTTCCTACCCTGGATAAATG
MBP-hKNG-domain D3	CATTTCTAGAGGGAAGGATTTTGTA	CTCTGCAGCTATGAGATCATTCCCAGTGGTTG

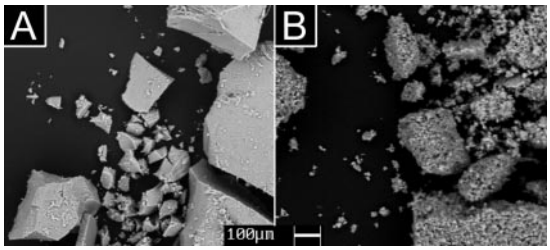

FIG. 1. **Ahsg-induced changes in morphology of BCP precipitate.** Scanning electron microscopy of BCP precipitate formed from a supersaturated solution of calcium (2.5 mM $CaCl_2$) and phosphate (1.8 mM KH_2PO_4) without (*A*) and with (*B*) added bovine Ahsg. The addition of 200 nM Ahsg induced a change in morphology of the precipitate from a compact to a brittle appearance indicating a strong interaction between the forming mineral phase and Ahsg.

solution (final concentration less than 50 µg/ml) into a vigorously stirred redox-refolding buffer (50 mM Tris, pH 8, 2 mM GSH, 0.2 mM GSSG, 1 M 3–(1-pyridino)-1-propane sulfonate, NDSB 201). The final yield of functional protein and its stability was greatly improved by adding NDSB 201 to the redox-refolding buffer. This solution was incubated for at least 1 day at room temperature to allow air oxidation of reduced protein. Using ultrafiltration, the initial buffer was replaced by 50 mM Tris/HCl, pH 7.4. The formation of aggregates during the refolding procedure was routinely analyzed by gel filtration chromatography using Superdex 200 and 75 gel filtration columns (Amersham Biosciences).

RESULTS

Inhibition of Basic Calcium Phosphate Precipitation by Ahsg—Our previous work has shown that Ahsg is highly effective *in vitro* to inhibit *de novo* formation of BCP (17). This inhibition was transient and lasted about 5–6 h at the conditions of our assay. The precipitation delay seems, however, sufficient to prevent generalized calcification *in vivo*. Our recent finding of severe systemic calcification of most soft tissues[2] in Ahsg-deficient mice validates the biological relevance of this concept. Here we asked how Ahsg interacts with the calcium and phosphate ions or the mineral nuclei to achieve inhibition.

Using scanning electron microscopy, we studied the influence of Ahsg on the morphology of the mineral precipitate. First, we analyzed the precipitate formed from a metastable calcium phosphate solution with or without added native bAhsg (Fig. 1). The exact nature of this precipitate is uncertain because of phase transitions. Therefore, we collectively address the precipitate formed as BCP, regardless of its exact chemical and crystallographic composition of variable proportions of amorphous calcium phosphate, octacalcium phosphate, and apatite. In the absence of bAhsg, copious amounts of BCP formed and appeared as a compact pellet (Fig. 1*A*). The addition of 200 nM bAhsg to the precipitation mixture barely reduced the amount of precipitate formed. However, the morphology of the BCP precipitate formed at this low concentration of bAhsg was changed into a loose, fluffy precipitate comprising small, 2–15-µm-sized aggregates (Fig. 1*B*).

A precipitation mix containing 10 µM bAhsg, the nominal serum concentration, was stable for many hours at 37 °C without any precipitate formation. Control incubations containing 10 µM BSA or no protein formed a clearly visible precipitate within 2 h under otherwise identical conditions. The precipitates of both controls were indistinguishable and were microcrystalline as judged by TEM (not shown). Next, the dialyzed supernatants were subjected to TEM analysis. Supernatants of precipitation mixtures, which had been incubated for 2 h at 22 or at 37 °C, respectively in the presence of 10 µM bAhsg contained spherical aggregates with a diameter of 30–150 nm (Fig. 2, *A* and *F*). The size and shape of the aggregates were independent of the order of $CaCl_2$ and Na_2HPO_4 addition. The precipitates were amorphous as judged by the lack of discrete diffraction patterns in TEM (Fig. 2*F*, *inset*). We termed these soluble, colloidal spheres "calciprotein particles" in analogy to the well established lipoprotein particles. The supernatant of both controls (with BSA and protein-free, respectively) did not contain any similar particles (not shown).

After 4 h of incubation at 37 °C, small crystalline needles started to grow on the surface of the calciprotein particles (Fig. 2*G*), but not at 22 °C (Fig. 2*B*). The fact that a diffraction pattern was obtained from samples incubated for 6 h at 37 °C indicated that crystallization had started (Fig. 2*H*, *inset*). A reduced temperature of 22 °C resulted in a delayed transformation of morphology (Fig. 2, *A–E*). After 23 h at 22 °C, crystallization of needles on the surface of spheres started to appear (Fig. 2*C*), similar in appearance to the samples harvested at 4 h and 37 °C (Fig. 2*G*). After 30 h at 37 °C, a solid BCP precipitate had formed. Small crystalline needles were present in the supernatant (Fig. 2*I*), whereas the precipitate consisted of large clusters of radially oriented needles with a diameter of about 450 nm (Fig. 2*J*). In summary, the transient inhibition of BCP precipitation by Ahsg relies on the formation of soluble colloidal spheres, "calciprotein particles," which progressively turn into an insoluble crystalline precipitate.

Next, we obtained information on the composition of the calciprotein particles by elemental mapping (Fig. 3). This procedure visualizes the electron energy loss at absorption edges characteristic of each element. Imaging of electrons with an energy loss corresponding to, for example, a calcium absorption edge will image the calcium-enriched regions of the specimen (19). Fig. 3 represents the elemental mapping of densely packed calciprotein particles harvested 2 h after the start of a precipitation reaction performed with 10 µM bAhsg at 37 °C. We show the elastically filtered image (mass density, Fig. 3*A*) and the phosphorus (Fig. 3*B*), the carbon (Fig. 3*C*), and the calcium (Fig. 3*D*) net distribution image of the same region. The elemental mapping indicates that all three elements were evenly distributed within the calciprotein particles.

We analyzed by dynamic light scattering (DLS) the speed of calciprotein particle formation in solution. First, we studied a solution of bAhsg without calcium and phosphate. We detected a major fraction (~99.5%) with a hydrodynamic radius (*rh*) of 4.2 nm corresponding to the Ahsg monomer and a small fraction (~0.5%) with *rh* = 55.4 nm, which we tentatively assigned to Ahsg aggregates (not shown). The addition of calcium resulted in an increase of the gyration radius by about 10%. Compared with the calcium phosphate- and Ahsg-containing samples (below), the scattering intensities were very low (Fig. 4). We observed a sharp rise in light scatter immediately after the addition of calcium and phosphate (Fig. 4). A slow, strongly scattering colloid matching the size of the calciprotein particles (*rh* = 40–50 nm) was detected in the solution, which we assigned to the emerging calciprotein particles. Within the first 1 h of incubation, a steep increase in the partial scattering intensity was measured (Fig. 4). During the following 19 h, the increase in intensity was moderate, yet continued. The hydrodynamic size still continued to grow after 1 day, but the intensity decreased (not shown). This is best explained by the complete sedimentation of the newly formed insoluble BCP precipitate.

Inhibition of BCP Precipitation by Proteins of the Cystatin Superfamily—To further analyze the structural requirements for efficient inhibition of BCP precipitation by Ahsg, we conducted a structure-function analysis of Ahsg-related proteins. We produced a series of mutated Ahsg fusion proteins as well as recombinant proteins related to Ahsg and measured their ability to inhibit BCP precipitation. To this end, we employed an established assay measuring co-precipitation of ^{45}Ca in a

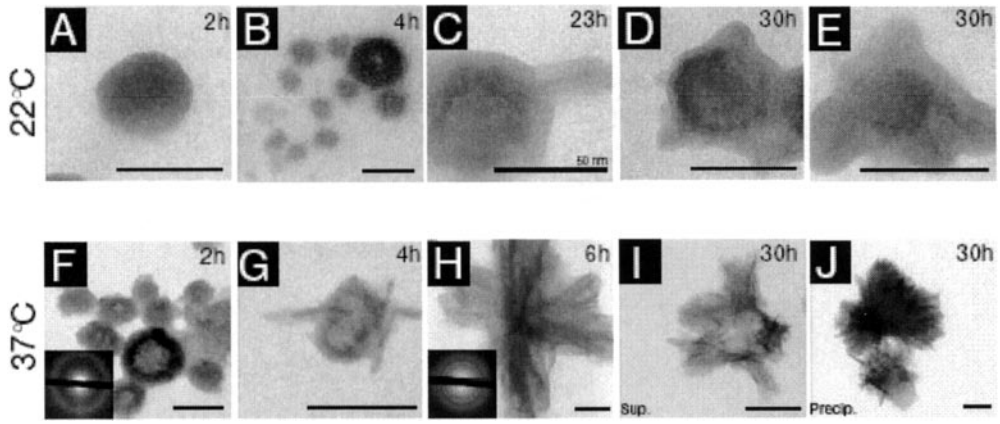

FIG. 2. **Growth and transformation of soluble calciprotein particles.** The inhibition of BCP precipitation by Ahsg is achieved by the formation of soluble colloidal complexes containing calcium, phosphate, and Ahsg. The calciprotein particles have a diameter of 30 to 150 nm (*A*, *B*, and *F*). Diffraction analysis indicated the temperature and time dependent transition of amorphous into crystalline BCP precipitate (*insets* in *F* and *H*). Radial growth of crystalline needles on the surface of the particles after 23 h at 22 °C (*C*) or after 4 h at 37 °C (*G*). After 30 h at 37 °C, crystalline but soluble needles were found in the supernatant (*I*). Electron dense crystals accumulated in the precipitate (*J*). The *scale bar* represents 100 nm, if not depicted otherwise.

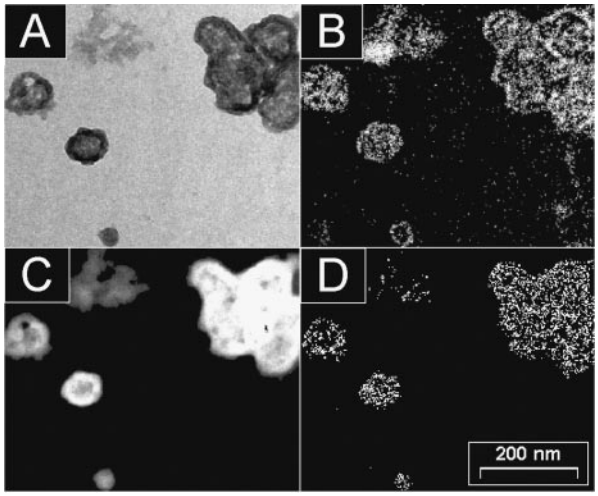

FIG. 3. **Electron filtering transmission electron microscopy analysis of the calciprotein particles.** *A–D*, the identical region of a representative sample. *A*, elastic bright field image; *B*, phosphorus elemental distribution image using the L2, 3-absorption edge at 200 eV; *C*, carbon elemental distribution image using the potassium absorption edge at 283 eV; *D*, calcium elemental distribution image using the L2, 3-absorption edge; both the Ca-L2 edge at 346 eV and the L3 edge at 350 eV contribute to this calcium mapping recorded at 350 eV. The three elements measured were evenly distributed within the calciprotein particles.

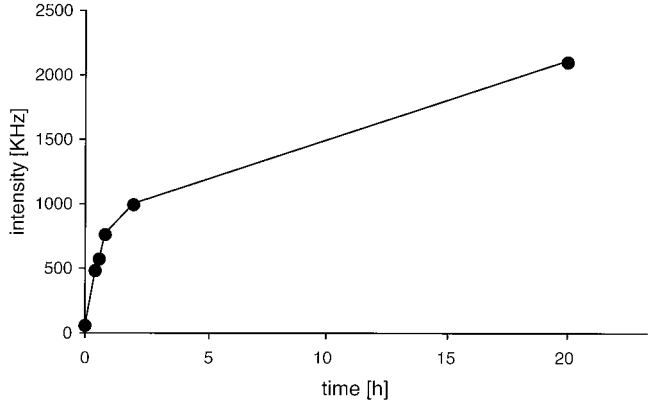

FIG. 4. **Monitoring calciprotein particle formation by DLS.** At a temperature of 20 °C a rapid DLS signal increase mirrored the formation and growth of amorphous calciprotein particles in Fig. 2, *A–B*. The slower increase of DLS signal observed thereafter reflects the subsequent crystallization depicted in Fig. 2, *C–E*.

buffered solution containing calcium, phosphate, and test protein (17). In this initial work, we had mapped the basal structural motif mediating the inhibition of spontaneous BCP precipitation to the amino-terminal cystatin-like Ahsg domain D1. Hence, we tested several related proteins of the cystatin superfamily containing structurally related cystatin-like protein domains. KNG contains three cystatin-like domains, HRG contains two, and Ahsg as well as its relative, the recently discovered FETUB (27), both contain two cystatin-like domains. We previously determined that HRG could inhibit precipitation, albeit with a 2-fold lower molar efficiency than Ahsg (28). We scanned for additional structural features that might contribute to the inhibition of calcification by Ahsg. It is known that post-translational modifications of mineral binding proteins, notably phosphorylation, influence their binding properties (7, 29). We and others reported that human Ahsg and rat Ahsg are transiently serine-phosphorylated (24, 25, 30). To assess the contribution of the resulting additional negative charge of mAhsg in the precipitation inhibition assay, we constructed the phosphorylation-mimicking mAhsg mutant mAhsg/4S>E by a site-directed mutagenesis of putative Ser (positions 120, 291, 294, and 296) phosphorylation sites with Glu. We expressed mAhsg, mAhsg/4S>E, human, mouse, and rat FETUB, and the three cystatin-like domains of hKNG in *Escherichia coli* as untagged or as FLAG-tagged proteins (data not shown) and as Myc-tagged fusion proteins with GST or with MBP. Generally, untagged or FLAG-tagged cystatin-like domains in our hands did not yield sufficient starting material for subsequent purification and functional testing. GST-fused proteins were more highly expressed (~15 mg of GST fusion protein/liter of LB medium) but tended to form insoluble inclusion bodies. Therefore, all recombinant proteins had to undergo an unfolding/refolding cycle in redox buffer before functional testing in the precipitation assay.

The *top section* of Fig. 5 shows the inhibition of BCP precipitation by negative control proteins, BSA and GST, and the positive control protein, bAhsg, at a concentration of 3 μM. Native serum bAhsg was most active in this assay, whereas BSA, GST, and MBP (17) did not significantly inhibit BCP precipitation under identical conditions.

Recombinant GST/MBP full-length mAhsg fused to GST or MBP proved active inhibitors of BCP precipitation like native bAhsg (Fig. 5). A comparison of the GST/MBP fusion proteins of mAhsg with the GST/MBP fusion proteins of mFETUB re-

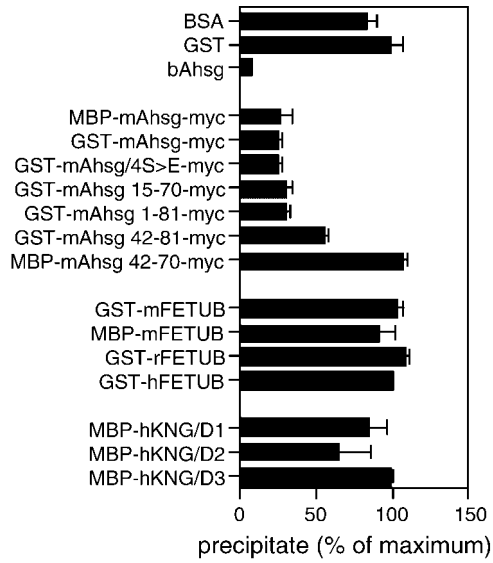

FIG. 5. **Inhibition of BCP formation by natural and mutated forms of cystatin-like domains of cystatin protein family members.** Recombinant forms of mAhsg; mFETUB, rFETUB, and hFETUB; and hKNG domains D1, D2, and D3 were expressed in *E. coli* as fusion proteins with MBP or GST as detailed under "Experimental Procedures." All proteins were tested at 3 μM final concentration. Results represent triplicate measurements ± S.E. *GST-mAhsg/4S>E-myc* denotes a mutant form of mouse Ahsg with serine residues 120, 291, 294, and 296 mutated to glutamic acid to mimic serine phosphorylation at these positions.

vealed that the FETUB was a much weaker inhibitor. Similarly, this observation applies to the GST fusions of human and rat FETUB. Likewise, none of the three MBP-fused cystatin-like domains of KNG proved to be an efficient inhibitor of BCP precipitation. We conclude that Ahsg, but not the related cystatin family members FETUB and KNG, is an efficient inhibitor of BCP precipitation. We observed no considerable difference between the activity of the GST-mAhsg/4S>E mutant and the wild type GST-mAhsg protein in their ability to inhibit BCP precipitation (Fig. 5). Therefore, serine phosphorylation of Ahsg does not seem to influence the inhibitory activity.

Next, we asked the question which minimal sequence within the cystatin-like Ahsg domain D1 confers the inhibition of BCP precipitation. To this end, we generated deletion mutants of the Ahsg domain D1 fused to GST. The resulting fusion proteins GST-mAhsg 1–81-Myc and GST-mAhsg 15–70-Myc were fully active in the BCP precipitation assay when compared with the full-length fusion proteins GST-mAhsg-Myc and MBP-mAhsg-Myc, respectively (Fig. 5). Shortening from the amino terminus (GST-mAhsg 42–81-Myc) and additionally from the C terminus (GST-mAhsg 42–70-Myc) caused a progressive loss of inhibitory activity (Fig. 5), which is completely lost in the mutant MBP-mAhsg 1–52 (17).

Structural Requirement for the Inhibition of BCP Precipitation by Cystatin-like Domains—To interpret the results obtained by the precipitation assay in a three-dimensional protein structure context, we aligned the protein sequences of 16 cystatin-like domains, namely of chicken egg white cystatin, human, mouse, and bovine Ahsg, human and mouse fetuin-B, human histidine-rich glycoprotein, and human kininogen using ClustalW software (Fig. 6). The alignments were manually adjusted to match the secondary structure elements identified in the crystal structure of chicken egg white cystatin (21) (Fig. 6*A*).

Based on the multiple sequence alignment (Fig. 6*D*), we generated models of each domain by comparative structure modeling using the published crystal structure of chicken egg white cystatin (21) as a template. Table II summarizes the sequence identity and similarity with the template sequence, the G-factors calculated by Procheck software (22), and the *Z* scores obtained by Prosa II software (23) as indicators of the accuracy of the modeled structures. According to these parameters, all models were free of steric clashes and well within the confines of theoretical structure prediction.

The segment of the mAhsg domain D1 model (Fig. 6, *B* and *C*), which adopts a β-sheet conformation when folded according to the known chicken egg white cystatin template structure (Fig. 6*A*) or when predicted by the sequence analysis software packages *PSIPRED* and *PHD* (31, 32) (data not shown), contains a remarkably high number of acidic amino acids, causing an extended negative surface charge (*red residues* in Figs. 6*C* and 7). In mAhsg D1, 6 out of 7 exposed residues in β-strands 2 and 3 of the four-pleated β-sheet are Asp or Glu, forming a contiguous acidic surface. These residues alternate with hydrophobic amino acids in a regular fashion, resulting in an asymmetric distribution of charge on opposing faces of the β-strands. Charged amino acids cluster on the exposed surface of the β-sheet facing the external milieu, whereas hydrophobic or uncharged amino acids cluster on the core side pointing toward the amino-terminal α-helix. No other cystatin-like domain analyzed showed a similarly regular pattern of charge distribution like mAhsg domain D1.

Next we scanned the modeled three-dimensional protein structure of each domain for features that would explain their differential activity in the BCP precipitation assay. Fig. 7 shows a compilation of identical views facing the extending β-sheets of all cystatin-like domains. The modeled structures are orientated in order to allow a top view of the four-pleated β-sheets. They illustrate striking differences in charge density on the extended β-sheets, which can also be detected in the protein sequence alignment (Fig. 6*D*). The alternating pattern of charges, which leads to a uniformly negative charge flanked by positive charges on the extended β-sheet of Ahsg D1 is absent or grossly distorted in the cystatin-like domains of chicken egg white cystatin, Ahsg domain D2, FETUB, and KNG (Fig. 7). The two cystatin-like domains of HRG show a coherent charged surface like Ahsg D1, but to a lesser extent. This may explain why hHRG inhibited the precipitation of BCP, albeit with a 2-fold lower molar efficiency than Ahsg (28), whereas none of the remaining cystatin-like domains inhibited BCP precipitation in this study (Fig. 5).

DISCUSSION

Fetuin/Ahsg is a potent inhibitor of BCP precipitation *in vitro* and *in vivo* (17, 33).[2] According to published literature, bovine fetuin/bAhsg binds one calcium ion tightly and five calcium ions more weakly (34). Based on a sequence alignment, it was proposed that Ahsg domain D1 harbors an EF-hand-like calcium binding motif, ^{92}EGDCDFQLLK^{101} (35). The amino acid positions 92–101 would, however, be located within β-strand 3 in our model of Ahsg domain D1 (Fig. 6), a configuration incompatible with a functional EF-hand. Therefore, EF-hand-like calcium binding is unlikely to mediate the efficient inhibition of precipitation of BCP caused by Ahsg. Also, on theoretical grounds, the simple binding of ionic calcium by Ahsg cannot be responsible for the inhibition of BCP precipitation. Considering the ion concentrations of the precipitation assay and assuming that one Ahsg molecule would bind six calcium ions, one can calculate that 3 μM Ahsg (the nominal concentration present in the precipitation mixture) would reduce the free calcium concentration to $6 \times 3 = 18$ μmol at best. This is insignificant compared with the millimolar concentration of calcium contained in the precipitation mixture and indeed most extracellular fluids of living animals. The solution

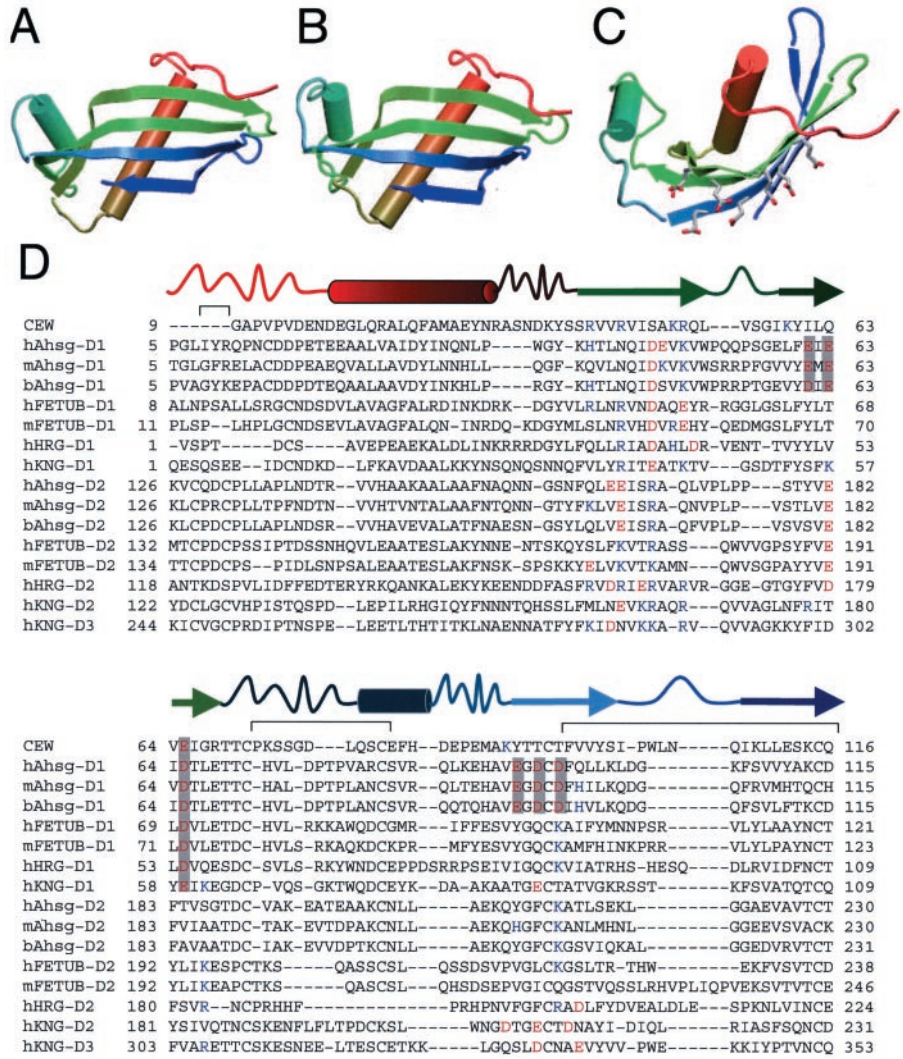

FIG. 6. **Sequence comparison of cystatin-like domains.** *A*, *schematic diagram* of chicken egg white cystatin (21). *B* and *C*, *schematic diagram* of mouse Ahsg domain D1 (mAhsg D1) modeled after *A*. *C*, a side view of *B* illustrating the arrangement of acidic amino acids on the four-pleated β-sheet. *D*, protein sequences of chicken egg white cystatin and the cystatin-like domains D1–3 of human, mouse, and bovine Ahsg (*h*, *m*, *bAhsg-D1* and *-D2*), human and mouse fetuin-B (*h*, *mFETUB-D1* and *-D2*), human histidine-rich glycoprotein (*hHRG-D1* and *-D2*), and human kininogen (*hKNG-D1-D3*) were aligned using ClustalW software (50). Alignments were manually corrected to match the boundaries of secondary structural elements (linearized *schematic diagram* and *color code* derived from *A*) and disulfide bridges (*brackets*) depicted *above* the sequence alignment. Positive charges are *blue*, and negative charges are *red*. Note that acidic amino acid residues Asp or Glu occupy nearly every exposed residue in the central β-strands 2 and 3 in human/mouse/bovine Ahsg domain D1 but not in any other cystatin-like domain depicted (*C* and *D*).

TABLE II
Quality assessment of modeled cystatin-like domains of mAhsg, mFETUB, hHRG, and hKNG

The percentage sequence identity and similarity reflects the quality of the alignment. PROSA II software returned *Z* scores as indicators of the combined conformational energy of all Cβ-Cβ interactions in each model. Low *Z* scores indicate a favorable conformation. Procheck software returned overall G-factors as an indicator of stereochemical quality of models. Both chemical bond angles and lengths were considered. All G-factors scored within the theoretically tolerated limits or better. High G-factors indicate favorable overall stereochemical geometry.

Cystatin-like domain	Identity/Similarity	*Z* score	Overall G-factor
	%		
mAhsg D1	15.7/24	−5.18	−0.2
mAhsg D2	17.6/24	−4.45	−0.5
mFETUB D1	21.3/16.7	−6.24	−0.3
mFETUB D2	25.5/17.9	−4.24	−0.4
hHRG D1	18.2/20.9	−5.35	−0.3
hHRG D2	22.2/21.3	−4.75	−0.3
hKNG D1	25.9/19.4	−6.87	−0.3
hKNG D2	20.4/21.3	−6.36	−0.2
hKNG D3	25.5/21.7	−5.18	−0.2

would still be supersaturated, and consequently, BCP precipitation would not be delayed. Therefore, the inhibition of BCP precipitation by Ahsg cannot be explained by a reduction of the ion product through calcium ion binding as in the case of albumin (36). Albumin does not have any extended β-sheet structure but is exclusively α-helical in nature (37). In the case of Ahsg, the arrangement of acidic amino acids in domain D1 and their folding into a defined array of charges on an extended β-sheet is, however, a crucial feature of effective inhibition of BCP precipitation. Based on the amount of calcium neutralized by Ahsg binding, we suggest that Ahsg binds BCP, not ionic calcium like serum albumin. Thus, both Ahsg and serum albumin contribute to extracellular calcium homoeostasis, albeit on a different level of complexity. In summary, extracellular proteins can bind calcium in three different ways illustrated in Fig. 8. Ahsg binds BCP, whereas albumin and the EF-hand protein SPARC/osteonectin bind free calcium with low and high affinity, respectively.

Our structure-function study of cystatin-like domains of Ahsg, FETUB, HRG, and KNG suggests that the β-sheet in Ahsg domain D1 is critically important for the inhibition of BCP precipitation. It forms a contiguous negatively charged, almost planar structure that is missing in Ahsg domain D2 and in all other modeled cystatin-like domains (Fig. 7). It is tempting to speculate that the acidic residues might occupy the phosphate lattice positions in apatite-like mineral through epitactic lattice matching. We hypothesize that the regularly spaced pattern of charges, characteristic of the extended β-sheet in Ahsg domain D1, is well suited to bind hydroxyapatite, especially at lattice planes with a high calcium content like the (001) plane. This binding mode is reminiscent of globular antifreeze proteins (38), which bind ice through several hydrogen bonding Asn and Gln residues arranged in a flat plane similarly arranged like the acidic residues in the ex-

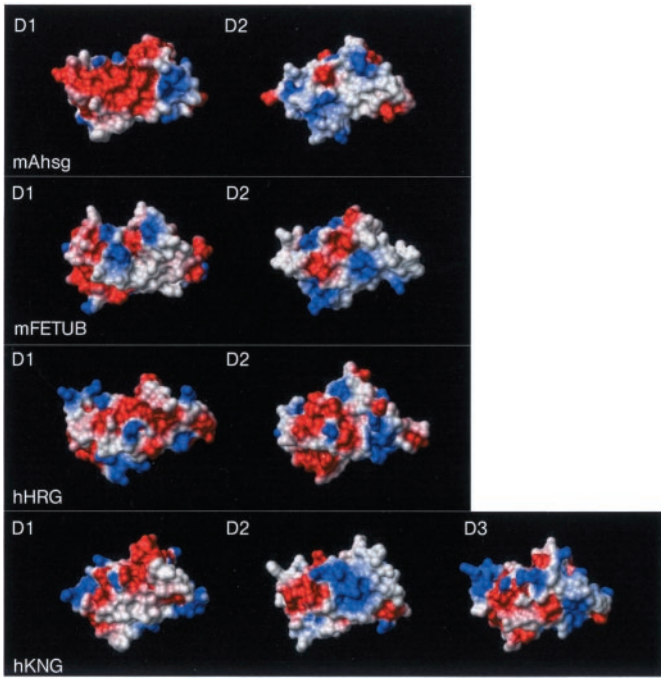

FIG. 7. **Surface charge distribution of cystatin-like protein domains.** Using the x-ray structure of chicken egg white cystatin (Protein Data Bank accession code 1CEW) (21) as a template, we modeled the cystatin-like domains of mAhsg, mFETUB, hHRG, and hKNG using Modeler4 software (20). The structures are orientated in order to allow a top view on the four-pleated β-sheets containing an extended acidic array depicted in *red* and basic residues in *blue*. Note that the accumulation of negative charge on the extended β-sheet of mAhsg D1 is absent in comparable cystatin-like domains.

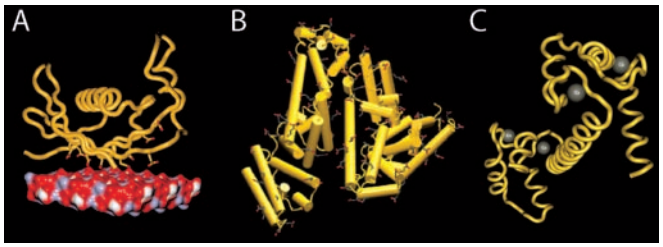

FIG. 8. **Calcium (phosphate) binding mechanisms of extracellular proteins Ahsg, serum albumin, and SPARC/osteonectin.** *A*, in Ahsg domain D1, surface binding of calcium is mediated by negative charges on the extended β-sheet of domain D1 (*top*) that might occupy PO_4 positions on the (001) face of apatite crystals (*bottom*), resulting in high affinity binding despite the relatively low serum concentration of Ahsg (10 μM). *B*, serum albumin binds calcium as counterions to numerous negatively charged amino acids (*red*) facing the external milieu. The high serum concentration of albumin (1 mM) causes high capacity calcium binding. *C*, high affinity binding is achieved by a functional EF-hand conformation. The calmodulin-like mode of calcium binding depicted here is established for few extracellular proteins (*e.g.* SPARC/osteonectin) (14).

tended β-sheet of Ahsg domain D1.

Structure-function information on the mechanism of calcification inhibition exists also for matrix-GLA protein, MGP. Targeted deletion of the MGP gene in mice results in lethal calcification of the aorta (13). Blocking of MGP glutamic acid γ-carboxylation by warfarin causes vascular calcification in young rats (39). Therefore, glutamate γ-carboxylation is regarded as critical for the function of MPG. The low solubility of MGP ($<$10 μg/ml) hampers structural research on this important inhibitor molecule, but the related bone-GLA protein/BGP/osteocalcin (40) has been analyzed by CD spectroscopy (41). In the α-helical conformation determined in this study, the spacing of the GLA residues in human BGP ((GLA)PRR(GLA)VC-

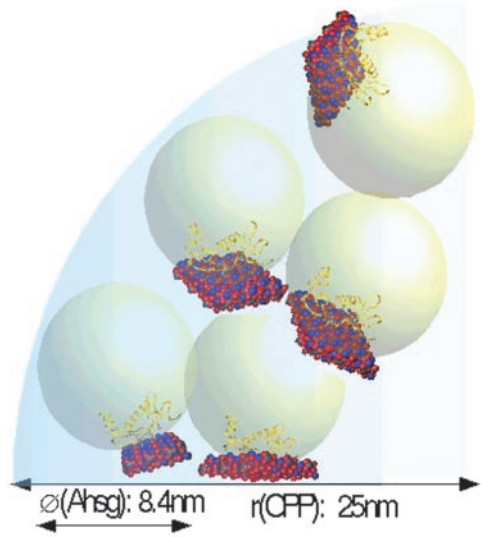

FIG. 9. **Hypothetical model of a calciprotein particle (large sphere quadrant) containing up to 100 globular Ahsg molecules (*small spheres*) with the cystatin-like domain D1 juxtaposed to nine apatite unit cells (minimodel from Fig. 8*A*).** Note that nine apatite unit cells arranged in a lattice of 3 $\times$ 3 closely match this number as well as the surface area of the extended β-sheet in Ahsg domain D1, which is drawn to scale.

(GLA)) results in the clustering of GLA residues on one side of the α-helix. This configuration may also exist in human MGP, which harbors two comparable sequence motifs ((GLA)RIR-(GLA) and (GLA)LNR(GLA)). Intriguingly, the interval of an α-helix of 540 pm corresponds to the distance of the Ca(I) ions in the (001) plane of the apatite structure permitting a tight binding of the GLA residue pairs to the Ca(I) ions on the mineral surface. Besides direct calcium binding, MGP may interfere with osteogenesis by regulating BMP-2 (42). Interestingly, Ahsg can likewise regulate osteogenesis by sequestering transforming growth factor-β and BMP-2 (43).

Here, we present a time-resolved TEM morphological study of direct physical calcification inhibition by Ahsg in *vitro* (Fig. 2) in the absence of osteogenic cells. Our study details the growth and transformation of the soluble precursors instead of the precipitate, which have been described (6, 26, 44, 45). The most important discovery of this study is that Ahsg forms transiently soluble, colloidal complexes with calcium and phosphate, which we termed calciprotein particles. At 37 °C and 10 μM Ahsg, which correspond to the normal serum temperature and Ahsg concentration, a BCP precipitate formed with a delay of at least 6 h. In biological terms, this suggests that Ahsg coating of BCP nuclei will delay the growth of insoluble crystals long enough to assure the mobilization and removal of otherwise insoluble calcium salts in the form of Ahsg containing calciprotein particles. We hypothesize that phagocytotic cells of the reticuloendothelial system (namely macrophages in spleen and liver and osteoclasts in bone marrow) will clear the calciprotein particles, thus mediating the recycling of extracellular calcium and phosphate from BCP. Corroborating this view, the total absence of Ahsg causes severe ectopic calcification of almost every soft tissue in Ahsg$-/-$ knockout mice,[2] and Ahsg deficiency is an independent predictor of vascular calcification in long term dialysis patients (15).

It remains to be determined whether the formation of calciprotein particles also plays a role in the dissolution of bone mineral. The removal of osteoclast bone resorption products involves transcytosis of vesicles containing bone mineral and bone matrix proteins (46, 47). Ahsg is a major noncollagenous protein in bone and teeth (48) and could therefore prevent the

precipitation of calcium salts during the transcytosis and thereafter. If this is so, calciprotein particles should be detectable in the bone remodeling compartment (49) and perhaps in the circulation. Our attempts to isolate Ahsg-, calcium-, and phosphate-containing calciprotein particles from blood of normo- and hypercalcemic mice were up until now unsuccessful. However, a high molecular weight complex containing calcium, phosphate, Ahsg/fetuin-A, and matrix-GLA protein was recently isolated in large amounts from the serum of etidronate-treated rats (51). It is very possible that this complex is identical with the calciprotein particles described in this study.

Our data suggest a novel mechanistic concept on the inhibition of generalized calcification by serum protein, namely by stabilization of soluble, colloidal particles containing calcium, phosphate, and the mineral-binding protein, Ahsg. We present a model calciprotein particle in Fig. 9. We arrived at this model by comparing the hydrodynamic radius of the Ahsg molecule (4.2 nm) estimated by dynamic light scattering (see Fig. 4) with the radius of 25 nm for an early calciprotein particle (Fig. 2*A*). A rough estimate of the number of globular Ahsg molecules required to fill the volume of a calciprotein particle arrives at ~100 Ahsg molecules. We adapted the stoichiometry of Ahsg-containing calciprotein from published literature (51), reporting an Ahsg/phosphate ratio of 7.6 mg/mg for soluble high molecular weight complex (in our model equal to early, soluble calciprotein particles (Fig. 2, *A* and *F*) and 3.4 mg/mg for the pelleted complex, respectively (late calciprotein particles-precipitate (Fig. 2, *I* and *J*)). Assuming a molecular mass of 50,000 for Ahsg and 1,000 for one apatite unit cell, this predicts a ratio of roughly 10 apatite unit cells (M_r 10,000) per Ahsg molecule for soluble, early calciprotein particles and ~22 apatite unit cells per Ahsg molecule for precipitating late calciprotein particles. Thus, on average, 9–12 apatite unit cells ($Ca_{10}(PO_4)_6(OH)_2$), corresponding to 90–120 calcium atoms and 54–72 phosphate ions, could be sequestered by one Ahsg molecule into a soluble complex aiding the transport of potentially insoluble BCP. This model is mechanistically similar to the well established lipoprotein particles, a colloid of lipid and protein. It should stimulate more research into the formation and recycling of BCP precipitates observed in many calcified lesions as well as novel approaches to the management of common calcification disorders for which there is currently no adequate therapy.

Acknowledgments—We thank Jaçek Gapinski for DLS analysis and Hermann Götz and Heinz Duschner for help with scanning electron microscopy.

REFERENCES

1. Kirschvink, J. L., Walker, M. M., and Diebel, C. E. (2001) *Curr. Opin. Neurobiol.* **11,** 462–467
2. Kröger, N., Lehmann, G., Rachel, R., and Sumper, M. (1997) *Eur. J. Biochem.* **250,** 99–105
3. Cha, J. N., Shimizu, K., Zhou, Y., Christiansen, S. C., Chmelka, B. F., Stucky, G. D., and Morse, D. E. (1999) *Proc. Natl. Acad. Sci. U. S. A.* **96,** 361–365
4. Addadi, L., and Weiner, S. (1985) *Proc. Natl. Acad. Sci. U. S. A.* **82,** 4110–4114
5. Shen, X., Belcher, A. M., Hansma, P. K., Stucky, G. D., and Morse, D. E. (1997) *J. Biol. Chem.* **272,** 32472–32481
6. Termine, J. D. (1988) *Ciba Found. Symp.* **136,** 178–202
7. Glimcher, M. J. (1990) *Biomaterials* **11,** 7–10
8. Busch, S., Dolhaine, H., Du Chesne, A., Heinz, S., Hochrein, O., Laeri, F., Podebrad, O., Vietze, U., Weiland, T., and Kniep, R. (1999) *Eur. J. Inorg. Chem.* 1643–1653
9. Neuman, W. F. (1980) in *Fundamental and Clinical Bone Physiology* (Urist, M. R., ed) pp. 83–107, Lippincott Co., Philadelphia
10. Schinke, T., McKee, M. D., and Karsenty, G. (1999) *Nat. Genet.* **21,** 150–151
11. Ho, A. M., Johnson, M. D., and Kingsley, D. M. (2000) *Science* **289,** 265–270
12. Nakamura, I., Ikegawa, S., Okawa, A., Okuda, S., Koshizuka, Y., Kawaguchi, H., Nakamura, K., Koyama, T., Goto, S., Toguchida, J., Matsushita, M., Ochi, T., Takaoka, K., and Nakamura, Y. (1999) *Hum. Genet.* **104,** 492–497
13. Luo, G., Ducy, P., McKee, M. D., Pinero, G. J., Loyer, E., Behringer, R. R., and Karsenty, G. (1997) *Nature* **386,** 78–81
14. Busch, E., Hohenester, E., Timpl, R., Paulsson, M., and Maurer, P. (2000) *J. Biol. Chem.* **275,** 25508–25515
15. Ketteler, M., Bongartz, P., Westenfeld, R., Wildberger, J., Mahnken, A., Böhm, R., Metzger, T., Wanner, C., Jahnen-Dechent, W., and Floege, J. (2003) *Lancet*, in press
16. Triffitt, J. T., Gebauer, U., Ashton, B. A., Owen, M. E., and Reynolds, J. J. (1976) *Nature* **262,** 226–227
17. Schinke, T., Amendt, C., Trindl, A., Pöschke, O., Müller-Esterl, W., and Jahnen-Dechent, W. (1996) *J. Biol. Chem.* **271,** 20789–20796
18. Walsh, D., Hopwood, J. D., and Mann, S. (1994) *Science* **264,** 1576–1578
19. Du Chesne, A. (1999) *Macromol. Chem. Phys.* **200,** 1813–1830
20. Sali, A., and Blundell, T. L. (1993) *J. Mol. Biol.* **234,** 779–815
21. Bode, W., Engh, R., Musil, D., Thiele, U., Huber, R., Karshikov, A., Brzin, J., Kos, J., and Turk, V. (1988) *EMBO J.* **7,** 2593–2599
22. Laskowski, R. A., MacArthur, M. W., Moss, D. S., and Thornton, J. M. (1993) *J. Appl. Crystallogr.* **26,** 283–291
23. Sippl, M. J. (1993) *Proteins* **17,** 355–362
24. Jahnen-Dechent, W., Trindl, A., Godovac-Zimmermann, J., and Müller-Esterl, W. (1994) *Eur. J. Biochem.* **226,** 59–69
25. Haglund, A. C., Ek, B., and Ek, P. (2001) *Biochem. J.* **357,** 437–445
26. Blumenthal, N. C. (1989) *Clin. Orthop. Relat. Res.* **247,** 279–289
27. Olivier, E., Soury, E., Ruminy, P., Husson, A., Parmentier, F., Daveau, M., and Salier, J. P. (2000) *Biochem. J.* **350,** 589–597
28. Schinke, T., Koide, T., and Jahnen-Dechent, W. (1997) *FEBS Lett.* **412,** 559–562
29. Raj, P. A., Johnsson, M., Levine, M. J., and Nancollas, G. H. (1992) *J. Biol. Chem.* **267,** 5968–5976
30. Auberger, P., Falquerho, L., Contreres, J. O., Pages, G., Le Cam, G., Rossi, B., and Le Cam, A. (1989) *Cell* **58,** 631–640
31. Rost, B., and Sander, C. (1993) *J. Mol. Biol.* **232,** 584–599
32. Jones, D. T. (1999) *J. Mol. Biol.* **292,** 195–202
33. Jahnen-Dechent, W., Schinke, T., Trindl, A., Müller-Esterl, W., Sablitzky, F., Kaiser, S., and Blessing, M. (1997) *J. Biol. Chem.* **272,** 31496–31503
34. Suzuki, M., Shimokawa, H., Takagi, Y., and Sasaki, S. (1994) *J. Exp. Zool.* **270,** 501–507
35. Brown, W. M., Dziegielewska, K. M., Saunders, N. R., Christie, D. L., Nawratil, P., and Müller-Esterl, W. (1992) *Eur. J. Biochem.* **205,** 321–331
36. Gilman, H., and Hukins, D. W. (1994) *J. Inorg. Biochem.* **55,** 21–30
37. He, X. M., and Carter, D. C. (1992) *Nature* **358,** 209–215
38. Jia, Z., DeLuca, C. I., Chao, H., and Davies, P. L. (1996) *Nature* **384,** 285–288
39. Price, P. A., Faus, S. A., and Williamson, M. K. (2000) *Arterioscler. Thromb. Vasc. Biol.* **20,** 317–327
40. Hauschka, P. V., Lian, J. B., Cole, D. E., and Gundberg, C. M. (1989) *Physiol. Rev.* **69,** 990–1047
41. Hauschka, P. V., and Carr, S. A. (1982) *Biochemistry* **21,** 2538–2547
42. Zebboudj, A. F., Imura, M., and Bostrom, K. (2002) *J. Biol. Chem.* **277,** 4388–4394
43. Szweras, M., Liu, D., Partridge, E. A., Pawling, J., Sukhu, B., Clokie, C., Jahnen-Dechent, W., Tenenbaum, H. C., Swallow, C. J., Grynpas, M. D., and Dennis, J. W. (2002) *J. Biol. Chem.* **277,** 19991–19997
44. Termine, J. D., Belcourt, A. B., Christner, P. J., Conn, K. M., and Nylen, M. U. (1980) *J. Biol. Chem.* **255,** 9760–9768
45. Suvorova, E. I., and Buffat, P. A. (1999) *J. Microsc.* (*Oxf.*) **196,** 46–58
46. Salo, J., Lehenkari, P., Mulari, M., Metsikko, K., and Vaananen, H. K. (1997) *Science* **276,** 270–273
47. Nesbitt, S. A., and Horton, M. A. (1997) *Science* **276,** 266–269
48. Triffitt, J. T. (1980) in *Fundamental and Clinical Bone Physiology* (Urist, M. R., ed) pp. 45–82, J. B. Lippincott Co., Philadelphia
49. Price, P. A., Caputo, J. M., and Williamson, M. K. (2002) *J Bone Miner. Res.* **17,** 1171–1179
50. Higgins, D. G., Thompson, J. D., and Gibson, T. J. (1996) *Methods Enzymol.* **266,** 383–402
51. Price, P. A., Thomas, G. R., Pardini, A. W., Figueira, W. F., Caputo, J. M., and Williamson, M. K. (2002) *J. Biol. Chem.* **277,** 3926–3934

Structural Basis of Calcification Inhibition by α_2-HS Glycoprotein/Fetuin-A: FORMATION OF COLLOIDAL CALCIPROTEIN PARTICLES

Alexander Heiss, Alexander DuChesne, Bernd Denecke, Joachim Grötzinger, Kazuhiko Yamamoto, Thomas Renné and Willi Jahnen-Dechent

J. Biol. Chem. 2003, 278:13333-13341.
doi: 10.1074/jbc.M210868200 originally published online January 29, 2003
